Mechanism of mediated alkali peroxide oxidation and triplet versus singlet oxygen formation

Yann K. Petit[1], Eléonore Mourad[1], Christian Prehal[1], Christian Leypold[1], Andreas Windischbacher[2], Daniel Mijailovic[1,3], Christian Slugovc[1], Sergey M. Borisov[4], Egbert Zojer[2], Sergio Brutti[5], Olivier Fontaine[6,7,8]* and Stefan A. Freunberger[1,8]*

[1] Institute for Chemistry and Technology of Materials, Graz University of Technology, Stremayrgasse 9, 8010 Graz, Austria

[2] Institute of Solid State Physics, Graz University of Technology Petersgasse 16, 8010 Graz, Austria

[3] University of Belgrade, Faculty of Technology and Metallurgy, Karnegijeva 4, 11120 Belgrade, Serbia

[4] Institute Analytical Chemistry and Food Chemistry, Graz University of Technology, Stremayrgasse 9, 8010 Graz, Austria

[5] Dipartimento di Chimica, Università di Roma La Sapienza. P.le A. Moro 5, 00185 Roma, Italy

[6] Institut Charles Gerhardt Montpellier, UMR 5253, CC 1502, Université Montpellier, Place Eugène Bataillon, 34095 Montpellier Cedex 5, France

[7] School of Energy Science and Engineering, Vidyasirimedhi Institute of Science and Technology (VISTEC), Rayong, 21210, Thailand

[8] IST Austria (Institute of Science and Technology Austria), Am Campus 1, 3400 Klosterneuburg, Austria

* e-mail: olivier.fontaine@vistec.ac.th, stefan.freunberger@ist.ac.at

Aprotic alkali metal–O_2 batteries function through the reversible filling of a porous cathode with alkali superoxides or peroxides. The two major obstacles to this chemistry occurring efficiently are the insulating nature of the products and parasitic reactions, which are caused by the highly reactive singlet oxygen ($^1O_2$). Redox mediators (RMs) are recognized to be key for improving rechargeability, however, how they affect $^1O_2$ formation is unclear, hindering strategies for their improvement. Here we clarify the mechanism of mediated peroxide and superoxide oxidation and thus explain how RMs either enhance or suppress $^1O_2$ formation. We show that charging commences with peroxide oxidation to a superoxide intermediate and that redox potentials above ~3.5 V vs. Li/Li^+ drive $^1O_2$ from superoxide oxidation while disproportionation always generates some $^1O_2$. We find that suppressing $^1O_2$ requires superoxide oxidation kinetics to be faster than the $^1O_2$ generation kinetics by disproportionation and the $^1O_2$ fraction from disproportionation to be small.

Oxygen redox chemistry is in the focus of forefront battery research with the aim to push energy storage beyond the limits of Li-ion batteries in terms of energy, sustainability and cost.[1-4] Non-aqueous alkali metal–O_2 cells use O_2 redox chemistry most directly by reducing O_2 at a porous, Li^+, Na^+, or K^+ electrolyte filled cathode to form alkali peroxides or superoxides[2-5]. Realizing high reversible capacities faces, however, two main challenges: First, the discharge products are insulators, which hampers filling the available pore space and removing it on charge[2,4-10]. Second and perhaps most vexing is parasitic chemistry, which decomposes cell components and causes poor rechargeability, efficiency, and cycle life[11-15].

The problems caused by the insulating nature of, e.g., Li_2O_2 and parasitic chemistry are interrelated and particularly severe on charge[2-7,9,11-14,16-20]. Deeply discharged O_2-cathodes are filled with Li_2O_2 particles with >100 nm in size[4,7,9,10,21,22]. Oxidizing them on charge is difficult even at low rates since charge transport becomes increasingly difficult, causing rising voltage and incomplete charge[4,7,20,21,23,24]. Parasitic reactions on discharge form side products such as Li_2CO_3 and Li carboxylates, which are hard to oxidize[4,12,13]. More of them form on charge with increasing rate as the voltage rises, which self-amplifies the processes[12,13,15,24]. Parasitic chemistry is now recognized to be significantly caused by the highly reactive singlet oxygen ($^1O_2$)[5,25-29].

To suppress parasitic chemistry, redox mediators (RMs) are now accepted to be key as they allow for recharging deeply discharged Li–O_2 or Na–O_2 cathodes at low voltages even at high rates[4,6,8,11,15-17,29-36]. A dissolved, reduced RM^{red} is oxidized at the cathode surface to RM^{ox}, which diffuses to M_2O_2 particles. These are oxidized to M^+ and O_2 with the mediator being itself reduced to RM^{red}. Mediators allow, in principle, charging at nearly zero overpotential and were investigated in wide variety for metal–O_2 cells[4,8,11,16,17,30-34,36]. However, RMs may also induce side reactions with the electrolyte[8,15,30,37]. Furthermore, since chemical oxidation of peroxides and superoxides in non-aqueous media by, e.g., chlorine or ferrocenium can generate $^1O_2$ (Refs. [38-42]), RMs may themselves produce $^1O_2$. Crucially, the mechanism of mediated alkali peroxide oxidation and pathways forming $^1O_2$ are unknown.

Here, we decipher the mechanism of mediated alkali peroxide and superoxide oxidation and identify the pathways towards $^1O_2$. $^1O_2$ forms by disproportionation of the superoxide intermediate and by mediated superoxide oxidation at redox potential >3.5 V vs Li/Li$^+$ (>3.3 V vs. Na/Na$^+$) with their relative kinetics governing the $^1O_2$ fraction. We show that superoxide oxidation kinetics slows down for RM potentials >3.2 V vs. Li/Li$^+$ and hence operates in the Marcus inverted region.

Results and discussion

We start with hypothesis of possible mediated oxidation mechanisms and pathways towards $^1O_2$. To prove them, we select mediators that span a wide range of redox potentials and we present $^1O_2$ and $^3O_2$ yields upon (su)peroxide oxidation. We then derive a general mechanism of mediated (su)peroxide oxidation, governed by mediator redox potential, the relative kinetics of electron transfer and disproportionation, and $^1O_2$ quenching.

Singlet oxygen evolution thresholds upon alkali (su)peroxide oxidation

Mediated alkali peroxide oxidation (M = Li, Na) has so far been described by the sum reaction[4,6,8,11,16,17,30-34,36]

$$M_2O_2 + 2\,RM^{ox} \xrightarrow{k_{app}} 2\,M^+ + 2\,RM^{red} + O_2 \qquad (1)$$

However, the individual steps need to be known to identify rate limitations and pathways towards $^1O_2$. We hypothesize that mediated oxidation may follow two possible pathways. First, direct two-electron oxidation according to equation (1). Second, analogous to electrochemical Li_2O_2 oxidation[2,5,19,21], a sequence of one-electron oxidation to form a superoxide species (denoted as MO_2 without implying the exact nature of the species)

$$M_2O_2 + RM^{ox} \xrightarrow{k_1} M^+ + RM^{red} + MO_2 \qquad (2)$$

followed by O_2 release through either a second one-electron oxidation

$$MO_2 + RM^{ox} \xrightarrow{k_2} M^+ + RM^{red} + O_2 \qquad (3)$$

or disproportionation. Thereby we consider three possible pathways towards $^1O_2$: First, disproportionation generates $^3O_2$ and $^1O_2$ according to

$$2\,MO_2 \xrightarrow{k_{DISP}} M_2O_2 + x\ {}^3O_2 + (1-x)\ {}^1O_2 \qquad (4)$$

The other two pathways are the electrochemical steps in equations (1) and (3), which can release $^1O_2$ beyond the thermodynamic threshold $E^{lim} = E^\circ + \Delta G(\,{}^1\Delta_g \leftarrow {}^3\Sigma_g^-)/zF$ (Fig. 1a). E^{lim} is ~3.54 V vs. Li/Li^+ for superoxide oxidation. Fig. 1a brings the M/M^+ scales (M = Li, Na, K) to a common scale based on their M/M^+ potentials vs. SHE. Since the standard potentials of the O_2/MO_2 couples are very similar on this scale, also the $^1O_2$ evolution thresholds E^{lim} for superoxide oxidation are very similar (dashed lines). Readily available KO_2 may therefore be used as a substitute for in pure form inaccessible LiO_2 (more detailed justifications are given in Supplementary Note 1). To clarify which of these possible steps prevail and how $^1O_2$ forms, we used a range of partly previously used mediators[8,16,17,30,34] with redox potentials ranging from just above the equilibrium potential of the O_2/Li_2O_2 couple at 2.96 V vs. Li/Li^+ to well beyond the $^1O_2$ generation threshold.

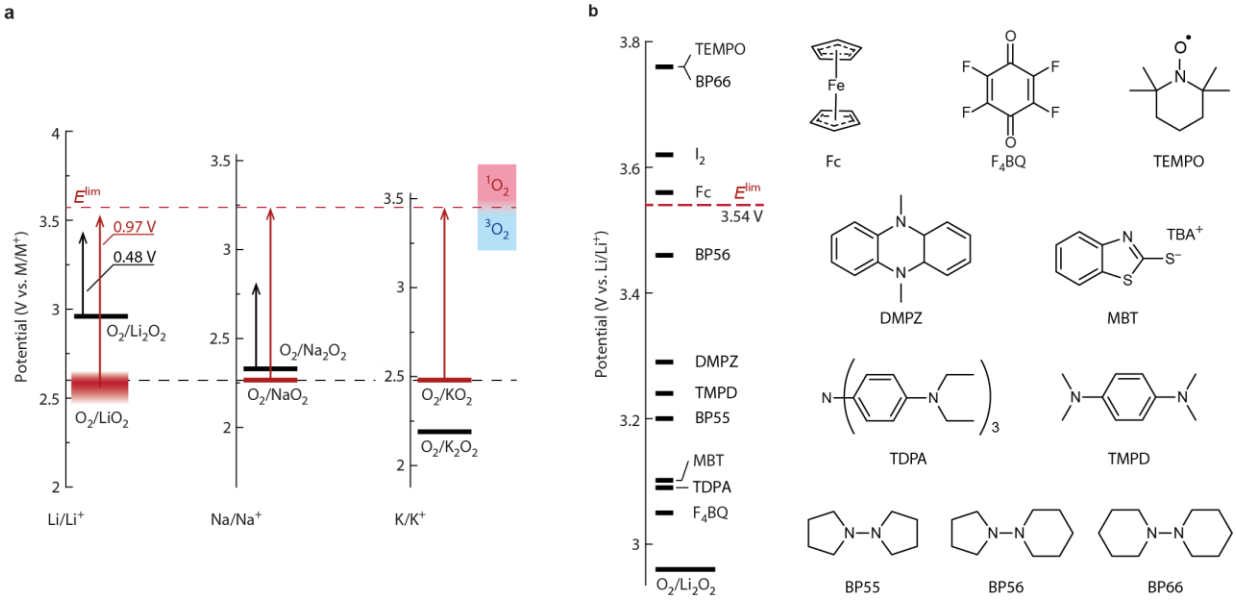

Figure 1 | Thermodynamics of alkali (su)peroxides, $^1O_2$ evolution thresholds and the used mediators. a, Standard potentials E^0 of the O_2/MO_2 and O_2/M_2O_2 redox couples on the M/M^+ scales with M = Li, Na, K. The scales are brought to a common scale based on their M/M^+ potentials vs. SHE. Thermodynamic thresholds for $^1O_2$ evolution $E^{\mathrm{lim}} = E° + \Delta G(\,^1\Delta_g \leftarrow \,^3\Sigma_g^-)/zF$. $\Delta G(\,^1\Delta_g \leftarrow \,^3\Sigma_g^-)$ is the Gibbs free energy difference between $^1O_2$ and $^3O_2$ (0.97 eV), z the transferred electrons, and F the Faraday constant[13,25,26,43]. Black arrows indicate E^{lim} for M_2O_2 oxidation via a hypothetical two-electron oxidation ($E° + 0.48$ V), red arrows E^{lim} for MO_2 oxidation ($E° + 0.97$ V). With $E°_{O_2/LiO_2}$ has been estimated to be ~2.57 V vs. Li/Li^+ (Ref. [44]) resulting in a threshold for $^1O_2$ generation of 3.54 V vs. Li/Li^+. **b**, The selected RMs, their abbreviations, and measured redox potentials on the Li/Li^+ scale. TBA^+ denotes tetrabutylammonium. Cyclic voltammograms of mediators not used before in metal–O_2 cells are shown in Supplementary Fig. 1 and 2. The red dashed lines in **a** and **b** indicate E^{lim} for superoxide oxidation.

Singlet oxygen and triplet oxygen yields

Figure 2 shows the $^3O_2$ and $^1O_2$ yields for the different RMs as a function of their redox potentials when reacted with Li_2O_2 or KO_2 (see Methods for experimental details). Values are given per two and one equivalents of RM^{ox} for Li_2O_2 or KO_2, respectively, according to the formally required equivalents per mol O_2. The mediators can be divided into three groups: 1) mediators with potentials ≳3.5 V that give significant $^1O_2$ yields (Fc, I_2, BP66, TEMPO); 2) mediators with a potential <3.5 V that evolve close to the expected total O_2 and small $^1O_2$ yields (BP55, TMPD, DMPZ, BP56); 3) low-voltage mediators that give significant $^1O_2$ yields (MBT, TDPA, F_4BQ). The total O_2 evolution is partly below the value

expected from the amount of RM^{ox}, particularly when oxidizing KO_2. This can be rationalized by imperfect $^1O_2$ trapping efficiency of DMA and that for some RMs only part of the RM^{ox} reforms RM^{red}, whilst a fraction of the RM forms side products (Supplementary Note 2).

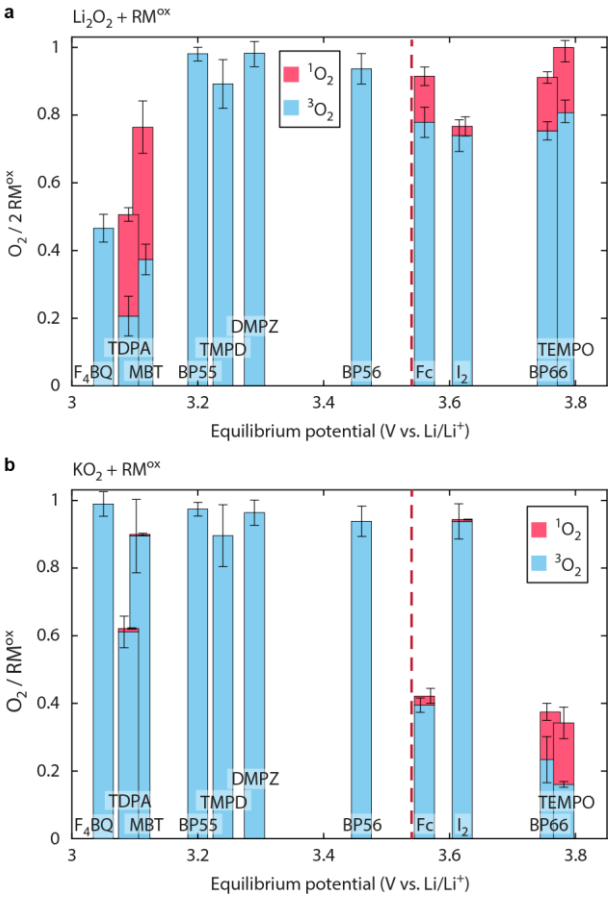

Figure 2 | Singlet and triplet oxygen evolution upon mediated peroxide and superoxide oxidation. a, **b**, Obtained $^3O_2$ and $^1O_2$ per two or one equivalents RM^{ox} when 10 mM RM^{ox} in TEGDME were added to an excess of Li_2O_2 (**a**) or KO_2 (**b**), respectively. $^3O_2$ and $^1O_2$ were measured by MS and DMA-to-DMA-O_2 conversion using HPLC, respectively. DMA is not compatible with F_4BQ and was hence not used there. Electrolytes contained either 0.1 M LiTFSI (**a**) or 0.1 M TBATFSI (**b**). The bars are positioned according to the equilibrium potentials of the $RM^{ox/red}$ couples and data are presented as mean ± s.d. The red dashed line indicates the thermodynamic threshold E^{lim} for $^1O_2$ evolution from MO_2 oxidation.

Considering first group 1, potentials ≳3.5 V, which exceed E^{lim}, partly explain significant $^1O_2$ yields for Fc, I_2, TEMPO, and BP66 as they could evolve $^1O_2$ via equation (3) from superoxide oxidation. The results are in accord with previous work observing $^1O_2$ from the reaction between O_2^- and oxidized

mediators with sufficiently high potentials such as Fc[40-42]. Disproportionation according to equation (4) is another source of $^1O_2$ [27,45].

At this point the question arises whether direct two-electron oxidation of Li_2O_2 according to equation (1) takes place as this could formally evolve $^1O_2$ above ~3.5 V vs. Li/Li$^+$ (Fig. 1a). Importantly, if direct oxidation were possible, then low-voltage mediators ($E^\circ_{\mathrm{RM}^{\mathrm{ox/red}}} < 3.5$ V) would evolve pure $^3O_2$ directly without passing via the superoxide intermediate. However, we show in Supplementary Note 3 that direct two-electron oxidation is unlikely. Therefore, peroxide oxidation passes via the superoxide intermediate, which in turn feeds with disproportionation a proficient $^1O_2$ source.

Turning to groups 2 and 3, mediators with redox potentials <3.5 V, thermodynamics in Fig. 1 suggests no $^1O_2$ to form by electrochemical oxidation (equations (1) and (3)). Indeed, negligible to little $^1O_2$ is observed for group 2 (BP55, TMPD, DMPZ, BP56). Group 3 (TDPA, MBT, F_4BQ) shows large $^3O_2$ deficiencies and significant $^1O_2$ yields. The possibility of $^1O_2$ forming with low-voltage mediators implies superoxide disproportionation to be the $^1O_2$ source. But also the virtual absence of $^1O_2$ with some mediators (group 2) suggests that the $^1O_2$ fraction from disproportionation may be suppressed. TDPA forms $^1O_2$ via a pathway involving TDPA^{2+}, highlighting that multistep mediators with a low first step are not necessarily save if they have steps >3.5 V (Supplementary Note 4). The general trend of $^1O_2$ yields found for mediated Li_2O_2 oxidation (Fig. 2a) is also found when Li_2O_2-packed carbon composite electrodes are electrochemically charged with electrolytes containing the mediators, confirming that the here described mechanism captures the mediated step in electrochemical cells (Supplementary Note 5).

Competing reactions kinetics

Disproportionation of superoxide intermediates according to equation (4) will always yield $^1O_2$ (Ref. [27]) even if mediated superoxide oxidation with $E^\circ_{\mathrm{RM}^{\mathrm{ox/red}}} < 3.5$ V will not. The $^1O_2$ yield hence results from competing kinetics of mediated oxidation and MO_2 disproportionation and the fraction of $^1O_2$ from disproportionation. To decipher the individual steps, we separately measured their rates as shown in

Fig. 3: (i) the reaction between Li_2O_2 and RM^{ox}, (ii) the reaction between KO_2 and RM^{ox}, and (iii) the rate of superoxide disproportionation.

The oxidation rates were measured by UV-Vis as detailed in the Methods. Compared to purely electrochemical methods, this has the advantage that possible side reactions not reforming RM^{red} could be spotted (Supplementary Note 6). The disproportionation rate was measured by immersing KO_2 pellets in Li^+ electrolyte and measuring the pressure increase in the closed vessel, Supplementary Fig. 7.

With respect to the apparent reaction rate $\nu_{\mathrm{app}} = k_{\mathrm{app}} \cdot c_{\mathrm{RM^{ox}}}$ between RM^{ox} and Li_2O_2 in Fig. 3a, we show in Supplementary Note 3 that it does not result from a direct two-electron oxidation (equation (1)). The apparent rate is hence a compound rate between the first one-electron extraction $\mathrm{M_2O_2} + \mathrm{RM^{ox}} \overset{k_1}{\rightarrow} \mathrm{M^+} + \mathrm{RM^{red}} + \mathrm{MO_2}$ and the following $\mathrm{MO_2} + \mathrm{RM^{ox}} \overset{k_2}{\rightarrow} \mathrm{M^+} + \mathrm{RM^{red}} + \mathrm{O_2}$, which competes with disproportionation. Comparing the kinetics of the latter two requires assuming a RM^{ox} concentration $c_{\mathrm{RM^{ox}}}$ to give the areal rate $\nu_2 = k_2 \cdot c_{\mathrm{RM^{ox}}}$, which may be compared to the areal disproportionation rate ν_{DISP} at the solid superoxide surface.

Figure 3b compares these rates. Superoxide oxidation rates show a maximum for BP55 at ~3.2 V and decreasing values as the redox potential (driving force) rises. Also k_{app} decreases in a similar way (Fig. 3a). Regarding the disproportionation, a previous report[27] has shown that weak Lewis acids such as tetrabutylammonium (TBA^+) markedly boost the rate and the $^1O_2$ fraction. We consider first the rate. To narrow down typical ranges of ν_{DISP} in presence of weakly Lewis acidic RM^{ox}, we measured ν_{DISP} in pure Li^+ electrolyte and a Li^+/TBA^+ mixture (Fig. 3b). This range of ν_{DISP} values allows rationalizing whether disproportionation or mediated superoxide oxidation dominates O_2 evolution. Accordingly, O_2 evolution is dominated by disproportionation for most mediators except for BP55. For all mediators, the combined kinetics of disproportionation and second electron transfer is much faster than the first one, meaning that the first electron extraction from peroxide is the rate-limiting step.

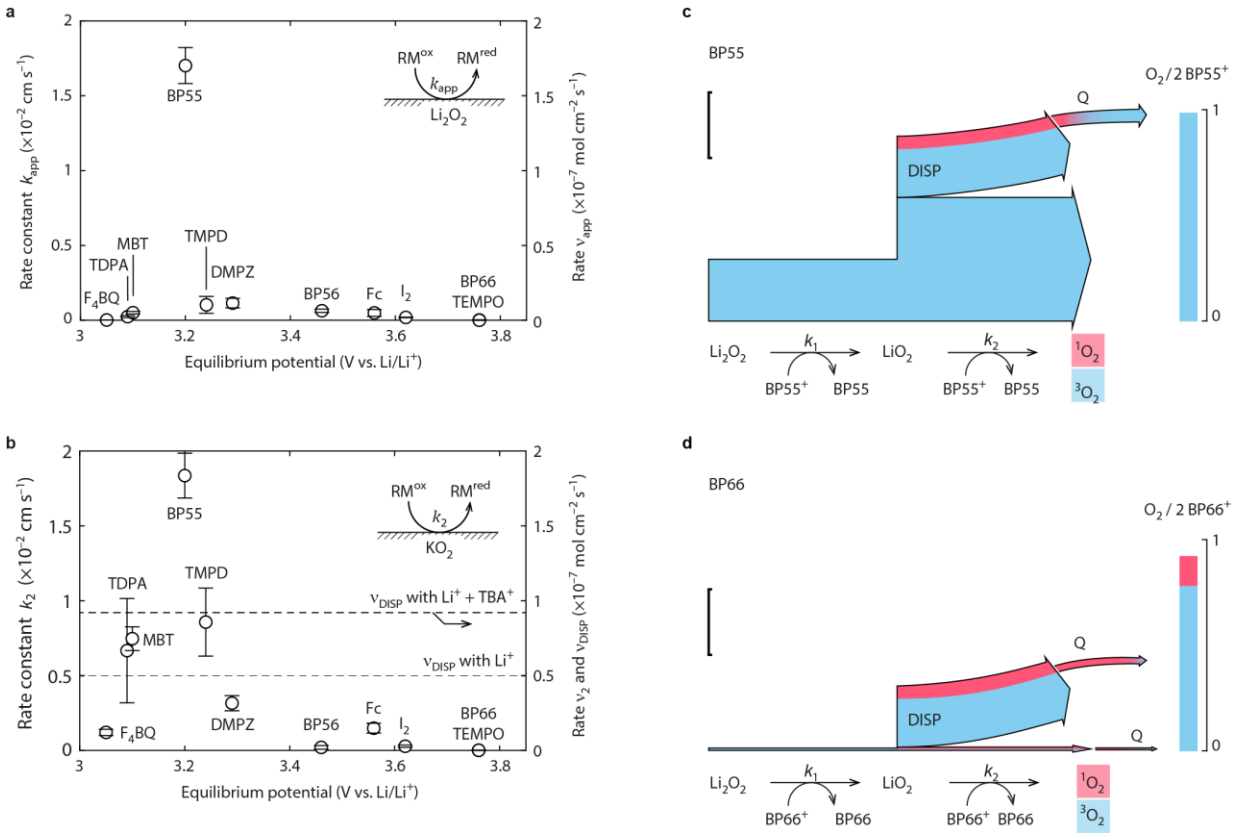

Figure 3 | Kinetics of mediated (su)peroxide oxidation and superoxide disproportionation. a, b, Rate constants k (left axis) and rates v (right axis) for the reaction between RM^{ox} and the Li_2O_2 surface (**a**) and the KO_2 surface (**b**) (data are presented as mean ± s.d., n ≥ 3). Rates are for a RM^{ox} concentration of 10 mM. The dashed lines in **b** indicate the disproportionation rate v_{DISP} of solid KO_2 in 0.1 M LiTFSI or 0.1 M LiTFSI plus 0.1 M TBATFSI, respectively. **c**, **d**, Sankey plots of relative rates during mediated Li_2O_2 oxidation for the examples of BP55 (**c**) and BP66 (**d**) to a superoxide intermediate (denoted as LiO_2 without implying its exact nature) and ongoing competing disproportionation (DISP) or mediated oxidation to yield $^1O_2$ (red) or $^3O_2$ (blue). The widths of the arrows are proportional to the rates (for 10 mM RM^{ox}) and the vertical scale bar corresponds to 1×10^{-7} mol·cm^{-2}·s^{-1}. $^1O_2$ quenching by the RM is denoted by Q. The $^3O_2$ and $^1O_2$ yields per 2 equivalent RM^{ox} are given at the right of each panel. Data are combined from Fig. 2 and 3a,b.

Turning to the changing $^1O_2$ fractions from disproportionation in presence of weak Lewis acids, the $^1O_2$ fraction was found to increase from ~3 to ~20% upon changing Li^+ for Li^+/TBA^+ electrolyte[27]. These resulted from the relative kinetics of singlet and triplet paths being influenced by the cations present. RM^{ox} are weak Lewis acids and will also affect the $^1O_2$ fraction from disproportionation as elaborated in Supplementary Note 7 and Extended Data Fig. 1. The $^1O_2$ fraction from disproportionation grows strongly with the RM^{ox} concentration and depends on the nature of the RM, reaching up to 90% $^1O_2$.

To more generally explain the $^3O_2$ and $^1O_2$ yields, Figs. 3b and d relate ν_1, ν_2, and ν_{DISP} for BP55 and BP66, which are prototypical cases for mediators below and above 3.5 V. The widths of the arrows are proportional to the rates of the individual steps and the bar graph at the right shows the shares of $^3O_2$ and $^1O_2$. Equivalent graphs for the other mediators are shown in Supplementary Fig. 8. The crucial outcome of this considerations is that (i) due to the fast disproportionation kinetics and (ii) considering that disproportionation always yields some $^1O_2$, $^1O_2$ is expected to be produced in all systems. Hence, suppressing $^1O_2$ requires superoxide oxidation kinetics to be faster than the kinetics of $^1O_2$ generation from disproportionation. For the $^1O_2$ fraction from disproportionation to be small, the RM^{ox} concentration must be small (Extended Data Fig. 1), which requires the charge transfer kinetics k_1 and k_2 to be fast (see Extended Data Fig. 2 and Supplementary Note 7 for a more detailed discussion). Furthermore, vanishing $^1O_2$ yields with BP55, TMPD, DMPZ and BP56 suggest that, besides favourable differences in the kinetic barriers between singlet and triplet reaction paths (Supplementary Note 8), an important step to suppress $^1O_2$ is the mediators' ability to quench $^1O_2$. Quenching rate constants of some mediators (BP55, TMPD, DMPZ, BP56, and I_2) are high enough to contribute to the small $^1O_2$ fractions (Supplementary Fig. 9).

Taken together, $^1O_2$ generation upon mediated peroxide oxidation is governed by the relative kinetics of superoxide oxidation and disproportionation, the fraction of $^1O_2$ from disproportionation (growing with RM^{ox} concentration), and the $^1O_2$ quenching ability of the mediator. Maximizing superoxide and peroxide oxidation kinetics is hence the most important handle to suppress $^1O_2$ generation for which the detailed analysis in the following provides mechanistic guidelines.

Electron transfer in the Marcus inverted region

Electron transfer rates slowing down as the driving force (mediator redox potential) increases beyond a certain value was strikingly observed in Fig. 3 for superoxide oxidation and similarly for k_{app}. Such

counterintuitive behaviour is predicted for homogeneous electron transfer by Marcus theory and termed the 'inverted region'[46,47]. Marcus' expression for the rate constant k_{ET} is given by

$$k_{\mathrm{ET}} = Z_{el} \cdot e^{\frac{-\Delta G^{\ddagger}}{R \cdot T}} \qquad (6)$$

where Z_{el} is the collision factor. The activation free energy is given by $\Delta G^{\ddagger} = (\Delta G^{\circ} + \lambda)^2/4\lambda$, where ΔG° is the driving force and λ the total reorganization energy, i.e., the energy required to change the nuclear configurations of reactants and solvent to the product states[46,47]. λ is composed of the 'inner' reorganization of the reactants, λ_{i} and the 'outer' reorganization of the solvent, λ_{o}. The latter depends hence on the electrolyte environment[37,46,47]. For superoxide oxidation it can be written as $\lambda = \lambda_{\mathrm{MO_2}} + \lambda_{\mathrm{RM^+}} = \lambda_{\mathrm{i,MO_2}} + \lambda_{\mathrm{o,MO_2}} + \lambda_{\mathrm{i,RM^+}} + \lambda_{\mathrm{o,RM^+}}$. Equation (6) predicts a maximum for k_{ET} when $-\Delta G^{\circ} = \lambda$ and barrier-less electron transfer as $\Delta G^{\ddagger}$ vanishes and decreasing k_{ET} with larger driving force. Equation (6) was derived for homogeneous electron transfer but does not apply to redox molecule reacting at metallic conductors[46,48]. With the latter, the inverted region disappears because of the near-continuum distribution of electrons around the Fermi level in metals, which creates intersections of a multitude of energy surfaces[48,49]. However, M_2O_2 and MO_2 are wide band-gap insulators. The distribution of occupied/unoccupied electronic states of an insulator can be approximated by a narrow Gaussian function and electron transfer involves discrete energy levels akin to free molecules, which may still justify using the formalism in equation (6) for homogeneous electron transfer between discrete energy levels. In support of this, Fig. 4 shows that equation (6) adequately fits the measured superoxide oxidation rates k_2 as a function of the driving force $-\Delta G^{\circ} = (E^{\circ}_{\mathrm{RM^{ox/red}}} - E^{\circ}_{\mathrm{O_2/LiO_2}})F$. Similarly, the trend for k_{app} is reproduced (Supplementary Fig. 11, Extended Data Fig. 2). Importantly, adequate description of rates by Marcus theory shows that physical meaning can be ascribed to Z_{el} and λ.

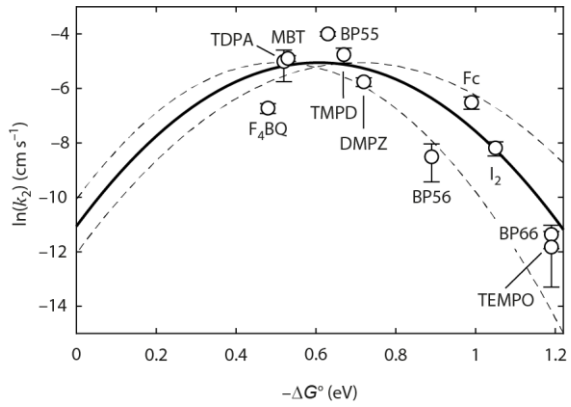

Figure 4 | Free energy dependence of superoxide oxidation kinetics. Plot of ln(k_2) versus $-\Delta G°$. The full line parabola is k_{ET} from the best fit of equation (6) which gives Z_{el} = 6.4·10^{-3} cm·s^{-1} and λ = 0.607 eV. The dashed parabolas are obtained with $\lambda \pm 0.1$ eV.

A central information from the adequacy of the fit is that chemically very different RMs can be described with a common value of $\lambda \sim 0.6$ eV (i.e., $E^{\circ}_{\mathrm{RM}^{\mathrm{ox/red}}} \sim 3.2$ V vs. Li/Li$^+$). This means that λ is dominated by the contributions of the oxide, which outweighs differences between contributions from the RMs. Or in other words $\lambda_{\mathrm{RM}^+} < \left(\lambda_{\mathrm{i,MO_2}} + \lambda_{\mathrm{o,MO_2}}\right)$, where the latter terms are associated with the M^+–O_2^- bond breaking and solvent reorganization from the MO_2 surface to $M^+_{(sol)}$ and $O_{2(sol)}$, respectively. Similar kinetics of chemically different RMs with similar redox potential supports this statement. Nevertheless differing reorganization energies between the RMs may in part account for deviations from the overall fit. To illustrate this, the dashed parabolas were drawn with the best fit $\lambda \pm$ 0.1 eV, which to a large extent captures deviations from predictions. Furthermore, deviations of measured kinetics from the overall fit in Fig. 4a will foremost also stem from differing collision factors Z_{el} (Refs. [47,49,50]).

Mediated alkali (su)peroxide oxidation mechanism

Figure 5 summarizes the mechanism of mediated alkali (su)peroxide oxidation and implications for $^1O_2$ evolution revealed here. Direct two-electron oxidation of Li_2O_2 or Na_2O_2 may be largely excluded. Instead, our data are consistent with, first, a one-electron oxidation to form a superoxide intermediate according to $\mathrm{M_2O_2} + \mathrm{RM^{ox}} \overset{k_1}{\rightarrow} \mathrm{M^+} + \mathrm{RM^{red}} + \mathrm{MO_2}$, which is the rate limiting step. With MO_2 we do

not imply any particular species as it may, for example, be a Li-deficient solid solution $Li_{2-x}O_2$ phase or dissolved $LiO_{2(sol)}$ as proposed before[2,5,18,19,21]. O_2 evolves by two competing pathways. First, a second one-electron oxidation $MO_2 + RM^{ox} \longrightarrow M^+ + RM^{red} + O_2$, which partly yields $^1O_2$ beyond the thermodynamic threshold $E^{lim} = E^0_{O_2/MO_2} + 0.97\ V$. This gives values for $E^{lim}_{^1O_2/MO_2}$ of 3.54 V, 3.24 and 3.45 vs. Li/Li^+, Na/Na^+, and K/K^+, respectively. Mediators beyond the threshold consistently show large $^3O_2$ deficiencies and significant $^1O_2$ yields. The second O_2 evolving pathway in case of Li–O_2 and Na–O_2 chemistry is disproportionation of the superoxide intermediate, which yields $^1O_2$ via $2\ MO_2 \longrightarrow M_2O_2 + x\ ^3O_2 + (1-x)\ ^1O_2$. Given that disproportionation always generates $^1O_2$, the extent to which low-voltage mediators (below the $^1O_2$ threshold) may suppress $^1O_2$ depends on three factors. First, the relative kinetics of mediated oxidation and $^1O_2$ formation from superoxide disproportionation. Second, since the $^1O_2$ fraction from disproportionation grows with RM^{ox} concentration, the mediated oxidation kinetics needs to be fast to keep the RM^{ox} concentration low. Third, the quenching ability of the mediator, which tends to be best with low voltage mediators.

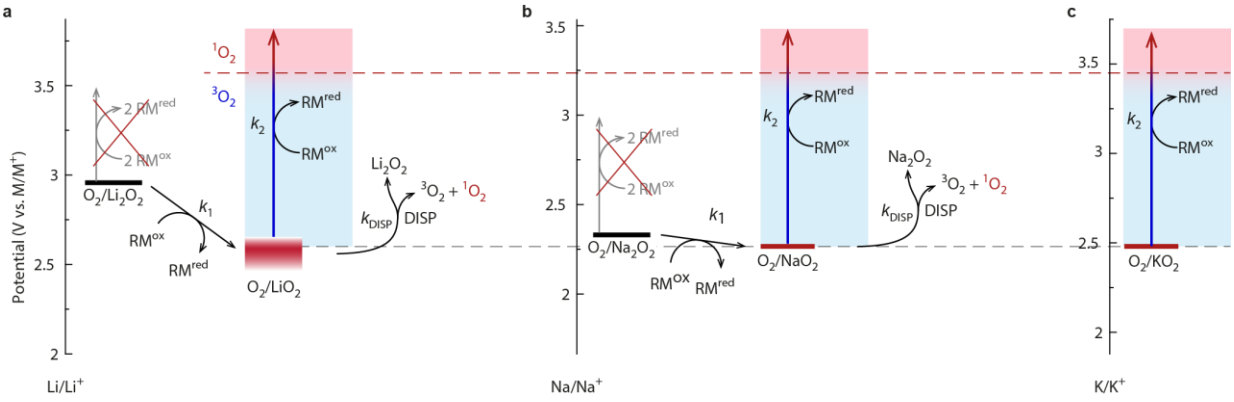

Figure 5 | Mediated alkali (su)peroxide oxidation mechanism. a-c, Oxidation mechanism of Li_2O_2 (**a**), Na_2O_2 (**b**), and KO_2 (**c**). The standard potentials E^0 of the O_2/MO_2 and O_2/M_2O_2 redox couples are shown on the M/M^+ scales (M = Li, Na, K). K_2O_2 is omitted because of KO_2 being the more stable species. The reaction arrows indicate the e^- extraction steps and their kinetics. First, a superoxide species (denoted as LiO_2 or NaO_2 without implying the exact nature of the species) is formed with kinetics k_1. This is followed by competing mediated second oxidation with kinetics k_2 or disproportionation (DISP, $2\ MO_2 \xrightarrow{k_{DISP}} M_2O_2 + x\ ^3O_2 + (1–x)\ ^1O_2$ for M = Li, Na) to yield $^1O_2$ (red) or $^3O_2$ (blue).

Conclusions

The mechanism of mediated alkali peroxide and superoxide oxidation is described and pathways leading to, in some cases substantial, $^1O_2$ generation are identified. This also suggests strategies to suppress $^1O_2$. Peroxide oxidation commences with the rate limiting step of a one-electron oxidation to a superoxide intermediate. Mediators with redox potentials $\gtrsim$3.5 V vs. Li/Li$^+$ drive $^1O_2$ from superoxide oxidation. Parallel disproportionation is found to dominate O_2 evolution for most mediators and always yields some $^1O_2$ and is hence the major source of $^1O_2$. The extent to which $^1O_2$ or $^3O_2$ evolve is governed by the relative kinetics of superoxide oxidation versus $^1O_2$ generation from disproportionation, the RM^{ox} concentration, and the mediator's $^1O_2$ quenching efficiency. The superoxide oxidation kinetics has a maximum at ~3.2 V vs. Li/Li$^+$ and decreasing values with higher potential. The apparent reaction rate between mediator and peroxide shows similarly decreasing rate. Remarkably, such behaviour is described by Marcus inverted region. The observation of an inverted region governing mediated (su)peroxide oxidation should enable strategies to find mediators that suppress $^1O_2$ generation.

References

1 Luo, K. et al. Charge-compensation in 3d-transition-metal-oxide intercalation cathodes through the generation of localized electron holes on oxygen. *Nat. Chem.* **8**, 684-691 (2016).

2 Lu, Y.-C. et al. Lithium-oxygen batteries: bridging mechanistic understanding and battery performance. *Energy Environ. Sci.* **6**, 750-768 (2013).

3 Choi, J. W. & Aurbach, D. Promise and reality of post-lithium-ion batteries with high energy densities. *Nat. Rev. Mater.* **1**, 16013 (2016).

4 Aurbach, D., McCloskey, B. D., Nazar, L. F. & Bruce, P. G. Advances in understanding mechanisms underpinning lithium–air batteries. *Nat. Energy* **1**, 16128 (2016).

5 Wang, Y. et al. A Solvent-Controlled Oxidation Mechanism of Li_2O_2 in Lithium–Oxygen Batteries. *Joule* **2**, 2364-2380 (2018).

6 Ko, Y. et al. Redox Mediators: A Solution for Advanced Lithium-Oxygen Batteries. *Trends in Chemistry* **1**, 349-360 (2019).

7 Gao, X., Chen, Y., Johnson, L. & Bruce, P. G. Promoting solution phase discharge in Li–O_2 batteries containing weakly solvating electrolyte solutions. *Nat. Mater.* **15**, 882–888 (2016).

8 Lim, H.-D. et al. Rational design of redox mediators for advanced Li–O_2 batteries. *Nat. Energy* **1**, 16066 (2016).

9 Aetukuri, N. B. et al. Solvating additives drive solution-mediated electrochemistry and enhance toroid growth in non-aqueous Li–O_2 batteries. *Nat. Chem.* **7**, 50-56 (2014).
10 Liu, T. et al. The Effect of Water on Quinone Redox Mediators in Nonaqueous Li–O_2 Batteries. *J. Am. Chem. Soc.* **140**, 1428-1437 (2018).
11 Liang, Z. & Lu, Y.-C. Critical Role of Redox Mediator in Suppressing Charging Instabilities of Lithium–Oxygen Batteries. *J. Am. Chem. Soc.* **138**, 7574-7583 (2016).
12 McCloskey, B. D. et al. Twin Problems of Interfacial Carbonate Formation in Nonaqueous Li–O_2 Batteries. *J. Phys. Chem. Lett.* **3**, 997-1001 (2012).
13 McCloskey, B. D. et al. Limitations in Rechargeability of Li–O_2 Batteries and Possible Origins. *J. Phys. Chem. Lett.* **3**, 3043-3047 (2012).
14 Liu, T., Kim, G., Casford, M. T. L. & Grey, C. P. Mechanistic Insights into the Challenges of Cycling a Nonaqueous Na–O_2 Battery. *J. Phys. Chem. Lett.* **7**, 4841-4846 (2016).
15 Burke, C. M. et al. Implications of 4 e^- Oxygen Reduction via Iodide Redox Mediation in Li–O_2 Batteries. *ACS Energy Lett.* **1**, 747-756 (2016).
16 Chen, Y. et al. Charging a Li–O_2 battery using a redox mediator. *Nat. Chem.* **5**, 489-494 (2013).
17 Bergner, B. J. et al. TEMPO: A Mobile Catalyst for Rechargeable Li–O_2 Batteries. *J. Am. Chem. Soc.* **136**, 15054-15064 (2014).
18 Lu, Y.-C. & Shao-Horn, Y. Probing the Reaction Kinetics of the Charge Reactions of Nonaqueous Li–O_2 Batteries. *J. Phys. Chem. Lett.* **4**, 93-99 (2012).
19 Kang, S., Mo, Y., Ong, S. P. & Ceder, G. A Facile Mechanism for Recharging Li_2O_2 in Li–O_2 Batteries. *Chem. Mat.* **25**, 3328–3336 (2013).
20 Wang, J. et al. Identifying Reactive Sites and Transport Limitations of Oxygen Reactions in Aprotic Lithium–O_2 Batteries at the Stage of Sudden Death. *Angew. Chem. Int. Ed.* **55**, 5201-5205 (2016).
21 Ganapathy, S. et al. Nature of Li_2O_2 Oxidation in a Li–O_2 Battery Revealed by Operando X-ray Diffraction. *J. Am. Chem. Soc.* **136**, 16335-16344 (2014).
22 Kwabi, D. G. et al. Controlling Solution-Mediated Reaction Mechanisms of Oxygen Reduction Using Potential and Solvent for Aprotic Lithium–Oxygen Batteries. *J. Phys. Chem. Lett.* **7**, 1204-1212 (2016).
23 Gao, X. et al. Phenol-Catalyzed Discharge in the Aprotic Lithium–Oxygen Battery. *Angew. Chem. Int. Ed.* **56**, 6539-6543 (2017).
24 Ottakam Thotiyl, M. M., Freunberger, S. A., Peng, Z. & Bruce, P. G. The Carbon Electrode in Nonaqueous Li–O_2 Cells. *J. Am. Chem. Soc.* **135**, 494-500 (2013).
25 Wandt, J. et al. Singlet Oxygen Formation during the Charging Process of an Aprotic Lithium–Oxygen Battery. *Angew. Chem. Int. Ed.* **55**, 6892-6895 (2016).
26 Mahne, N. et al. Singlet oxygen generation as a major cause for parasitic reactions during cycling of aprotic lithium–oxygen batteries. *Nat. Energy* **2**, 17036 (2017).
27 Mourad, E. et al. Singlet oxygen from cation driven superoxide disproportionation and consequences for aprotic metal–O_2 batteries. *Energy Environ. Sci.* **12**, 2559-2568 (2019).
28 Schafzahl, L. et al. Singlet Oxygen during Cycling of the Aprotic Sodium–O_2 Battery. *Angew. Chem. Int. Ed.* **56**, 15728-15732 (2017).
29 Liang, Z., Zou, Q., Xie, J. & Lu, Y.-C. Suppressing singlet oxygen generation in lithium–oxygen batteries with redox mediators. *Energy Environ. Sci.* (2020).
30 Park, J.-B. et al. Redox Mediators for Li–O_2 Batteries: Status and Perspectives. *Adv. Mat.* **30**, 1704162 (2018).
31 Pande, V. & Viswanathan, V. Criteria and Considerations for the Selection of Redox Mediators in Nonaqueous Li–O_2 Batteries. *ACS Energy Lett.* **2**, 60-63 (2017).
32 Chen, Y., Gao, X., Johnson, L. R. & Bruce, P. G. Kinetics of lithium peroxide oxidation by redox mediators and consequences for the lithium–oxygen cell. *Nat. Commun.* **9**, 767 (2018).
33 Gao, X. et al. A rechargeable lithium–oxygen battery with dual mediators stabilizing the carbon cathode. *Nat. Energy* **2**, 17118 (2017).

34 Kundu, D., Black, R., Adams, B. & Nazar, L. F. A Highly Active Low Voltage Redox Mediator for Enhanced Rechargeability of Lithium–Oxygen Batteries. *ACS Central Sci.* **1**, 510-515 (2015).

35 Chase, G. V. et al. Soluble oxygen evolving catalysts for rechargeable metal-air batteries. US Patent App. 13/093,759 (2011).

36 Landa-Medrano, I. et al. Redox mediators: a shuttle to efficacy in metal–O_2 batteries. *J. Mat. Chem. A* **7**, 8746-8764 (2019).

37 Leverick, G. et al. Solvent-Dependent Oxidizing Power of LiI Redox Couples for Li–O_2 Batteries. *Joule*.

38 Li, Q. et al. A Spectroscopic Study on Singlet Oxygen Production from Different Reaction Paths Using Solid Inorganic Peroxides as Starting Materials *Bull. Korean Chem. Soc.* **28**, 1656-1660 (2007).

39 Qingwei, L. et al. Singlet Oxygen Production in the Reaction of Potassium Superoxide with Chlorine. *Chem. Lett.* **36**, 496-497 (2007).

40 Mayeda, E. A. & Bard, A. J. Production of singlet oxygen in electrogenerated radical ion electron transfer reactions. *J. Am. Chem. Soc.* **95**, 6223-6226 (1973).

41 Senthil Kumar, S. & Bard, A. J. Background Emission of Electrogenerated Chemiluminescence during Oxidation of Tri-*n*-propylamine from the Dimeric $^1\Delta_g$ State of O_2. *Anal. Chem.* **85**, 292-295 (2013).

42 Ando, W. et al. Formation of sulfinyl oxide and singlet oxygen in the reaction of thianthrene cation radical and superoxide ion. *J. Am. Chem. Soc.* **102**, 4526-4528 (1980).

43 Hassoun, J., Croce, F., Armand, M. & Scrosati, B. Investigation of the O_2 Electrochemistry in a Polymer Electrolyte Solid-State Cell. *Angew. Chem. Int. Ed.* **50**, 2999-3002 (2011).

44 Kwabi, D. G. et al. Experimental and Computational Analysis of the Solvent-Dependent O_2/Li^+-O_2^- Redox Couple: Standard Potentials, Coupling Strength, and Implications for Lithium–Oxygen Batteries. *Angew. Chem. Int. Ed.* **55**, 3129-3134 (2016).

45 Pierini, A., Brutti, S. & Bodo, E. Superoxide anions disproportionation induced by Li^+ and H^+: pathways to $^1O_2$ release in Li–O_2 batteries. *ChemPhysChem* **21**, 2060-2067 (2020).

46 Marcus, R. A. Electron transfer reactions in chemistry. Theory and experiment. *Rev. Mod. Phys.* **65**, 599-610 (1993).

47 Savéant, J.-M. *Elements of molecular and biomolecular electrochemistry*. (John Wiley & Sons, 2006).

48 Henstridge, M. C., Laborda, E., Rees, N. V. & Compton, R. G. Marcus–Hush–Chidsey theory of electron transfer applied to voltammetry: A review. *Electrochim. Acta* **84**, 12-20 (2012).

49 Feldberg, S. W. & Sutin, N. Distance dependence of heterogeneous electron transfer through the nonadiabatic and adiabatic regimes. *Chem. Phys.* **324**, 216-225 (2006).

50 Fawcett, W. R. *Liquids, Solutions, and Interfaces – From Classical Macroscopic Descriptions to Modern Microscopic Details*. (Oxford University Press, 2004).

Acknowledgements

S.A.F. is indebted to the European Research Council (ERC) under the European Union's Horizon 2020 research and innovation programme (grant agreement No 636069) as well as IST Austria. O.F thanks the French National Research Agency (STORE-EX Labex Project ANR-10-LABX-76-01). The authors thank R. Saf for help with the MS, J. Schlegl for manufacturing instrumentation, M. Winkler of Acib GmbH, G. Strohmeier and R. Fürst for HPLC measurements, and S. Mondal and S. Stadlbauer for kinetic measurements.

Author Contributions

S.A.F., Y.K.P., E.M., C.L., C.P., D.M., and S.M.B. performed experiments. S.B., A.W., and E.Z. did DFT calculations. C.S. helped with synthesis. O.F. contributed to data interpretation. S.A.F. conceived and directed the research, set up and performed all types of experiments, analysed the results, and wrote the manuscript. All authors contributed to the discussion and interpretation of the results.

Competing Financial Interests

The authors declare no competing financial interests

Methods

Materials. Lithium bis(trifluoromethane)sulfonimide (LiTFSI, 99.9%, Solvionic) was dried under reduced pressure for 24 h at 140°C. 2,2,6,6-tetramethyl-1-piperidinyloxy(TEMPO), tris[4-(diethylamino)phenyl]amine (TDPA), *N,N,N',N'*-tetramethyl-*p*-phenylenediamine (TMPD), 2,2′-dithiobis(benzothiazole) (MBT_2), thiobis(benzothiazole) (MBTH), ferrocene (Fc), I_2, 5,10-dihydro-5,10-dimethylphenazine (DMPZ), N-methyl phenothiazine (MPT), and tetrafluorobenzoquinone (F_4BQ) were from Sigma Aldrich. MBT_2, MPT, F_4BQ, and I_2 were recrystallized from ethanol or sublimated, respectively. Ethylene glycol dimethyl ether (DME, >99.0%, Aldrich) and tetraethylene glycol dimethyl ether (TEGDME, ≥99%, Aldrich) were dried over lithium, distilled under Ar and further dried and stored over activated molecular sieves. The water content was determined by Karl-Fisher titration and found to be below 5 ppm. 9,10-Dimethylanthracene (DMA, >98.0 %, Aldrich) was recrystallized from ethanol and its purity confirmed by ^{1}H-NMR spectroscopy and HPLC analysis.

Lithium peroxide (Li_2O_2) was synthesized as described previously[24]. Its purity was confirmed by XRD and ATR-IR spectroscopy. Formic acid, water, and acetonitrile as HPLC solvents were from Fluka, Sigma, and VWR, respectively. $LiFePO_4$ was from MTI.

Synthesis. Oxidized mediators were obtained by oxidizing the reduced forms using one equivalent nitrosonium tetrafluoroborate ($NOBF_4$, Aldrich) in CH_3CN during 3 hours under agitation. They were purified by precipitation in cold ether, filtration, and drying under vacuum at 30 °C for 12 hours. Highly pure Li_2O_2 was synthesized as follows. All operations were performed in an Ar filled glove box. Freshly cut Li metal was dissolved in 5-fold excess of ultra-pure water (Millipore, 18.2 MΩ) that was degassed by an Ar flow. LiOH was obtained by drying at 120°C under vacuum. Its purity was confirmed by the carbonate/carboxylate analysis[51]. The LiOH was converted into Li_2O_2 with 1.85-fold excess of 30 % H_2O_2. After stirring for 30 min, the water was removed and the Li_2O_2 was dried at 120°C for 12 h under vacuum. Identity and purity was confirmed by XRD, FTIR, and carbonate/carboxylate analysis[51]. To obtain Li_2O_2 that could be pressed into self-standing pellets, PTFE suspension (60% in water, Aldrich) was added to the LiOH in an extent to get 90/10% w/w Li_2O_2/PTFE. Syntheses of MBTLi, BP55, BP56 and BP66 are detailed in the Supplementary Methods.

Electrochemistry and analysis. Electrochemical experiments were run on a potentiostat/galvanostat (SP-300 or MPG-2, Bio-Logic). Cyclic voltammograms were recorded in a three-electrode arrangement with glassy carbon disc working electrode (3 mm) or a gold UME (12.5 μm), a Pt wire counter electrode and partially delithiated $LiFePO_4$ in 0.1 M $LiClO_4$/TEGDME behind a vycor glass frit as reference electrode inside a glass cell with PTFE lid. The reference was checked versus Fc^+/Fc. The cells were run inside an Ar filled glovebox and purged with high-purity Ar. For rotating disc measurements, a Princeton Applied Research device with in-house made 5 mm GC disc was used. The $LiFePO_4$ counter electrode was separated from the electrolyte using a Li-conducting ceramic (Ohara), glued into a PEEK cell using silicon glue (RS), the $LiFePO_4$ reference electrode was separated by a Vycor glass frit (ALS). Metal-O_2 cells with integrated pressure transducer were of the type PAT-Cell-Press (EL-Cell GmbH, Hamburg, Germany) with custom modified cathode plunger. The atmosphere was pure O_2 at a pressure of ~1.2 bar and the cell kept in an incubator at 20±0.1 °C. Working electrodes were made by mixing

Ketjen Black carbon black with PTFE (9/1 w/w) using isopropanol to obtain a paste which was then rolled on a glass plate to 100 µm thickness. The punched electrodes were dried on air, then washed with 1/1 water/acetone mix and dried overnight at 200 °C in vacuum. Li_2O_2 loaded electrodes were made by mixing Ketjen Black carbon black with PTFE (9/1 w/w) with isopropanol and water to obtain a thin slurry, which was thinly spread on a glass plate, dried on air, scratched off and dried overnight at 200 °C in vacuum. This powder was mixed inside a glove box with Li_2O_2 (1/1 w/w with respect to C) and rolled to 100 µm thick electrodes. The $LiFePO_4$ counter electrode was separated from the working electrode using a PEEK insert with a Li-conducting ceramic (Ohara) glued in using silicon glue (RS).

Singlet and triplet oxygen yields were measured by injected solutions of 10 mM RM^{ox} in tetraethyleneglycol dimethylether (TEGDME) into a closed vessel containing an excess of Li_2O_2 or KO_2. The sample setup was similar to the one described in Ref. [51] and consisted of a glass vial with a volume of 7 mL equipped with a stirring bar. A PEEK plug with glued in PEEK tubes and a septum was sealed against the glass vial with a flat rubber seal. Reagents were added through a septum using a gas tight syringe (Hamilton). All solutions were degassed with N_2 to remove dissolved CO_2 and O_2. The head space was purged with 5 $mL \cdot min^{-1}$ Ar 6.0 to a mass spectrometer (MS) to quantify the evolved $^3O_2$. The mass spectrometry (MS) setup was built in-house and described in more detail in Ref [26]. The solutions also contained 30 mM 9,10-dimethylanthracene (DMA) to probe $^1O_2$ formation[26]. DMA reacts selectively with $^1O_2$ to its endoperoxide (DMA-O_2) and the DMA-to-DMA-O_2 conversion High-performance liquid chromatography (HPLC) was used to determine the degree of the DMA-to-DMA-O_2 conversion as described in more detail Ref. [26]. While the reaction between DMA and $^1O_2$ is fast, the $^1O_2$ amount determined from DMA-to-DMA-O_2 conversion has to be considered as a lower limit since competing $^1O_2$ decay routes may prevail. The O_2 evolution rate during the disproportionation reaction was measured using a high-precision pressure transducer (Omega, PAA35X) connected to the closed vessel instead of the MS. Reagents were added with a gas tight syringe through glued-in tubing.

UV-Vis absorption spectra were recorded on a Cary 50 spectrophotometer (Varian) or V-770 (Jasco). Reaction kinetics were measured by operando UV-vis in a 1 cm quartz cuvette (Hellma) with a gas tight injection lid. Li_2O_2/PTFE powder (90/10 % w/w)) or pure KO_2 powder, respectively, were pressed with

a 7 mm die set and a hand press (PIKE) to ~0.5 mm thick pellets in an Ar-filled glove box. A pellet was placed in a PTFE frame in the cuvette with magnetic stirrer on top and RM^{ox} solution was injected using a gas tight syringe (Hamilton). Data are shown in Supplementary Figs. 3 to 6. For the slowest kinetics, the reaction kinetics was additionally measured by following the pressure evolution upon bringing KO_2 or Li_2O_2 powder in contact with RM^{ox} solution in TEGDME. For Li_2O_2, the solution contained additionally 0.1 M LiTFSI and the rate was calculated taking into account the fraction of $^3O_2$ evolved. To establish relative surfaces of the pellet and the powders, the latter were also measured using $DMPZ^+$ and $TEMPO^+$. The quenching efficiency was measured by monitoring the disappearance rate of the $^1O_2$ trap DMA in presence or absence of the quenchers during continuous photochemical $^1O_2$ generation as frequently used in the literature[52]. Details are described in Ref. [53].

References

51 Schafzahl, B. et al. Quantifying Total Superoxide, Peroxide, and Carbonaceous Compounds in Metal–O_2 Batteries and the Solid Electrolyte Interphase. *ACS Energy Lett.* **3**, 170-176 (2017).

52 Wilkinson, F., Helman, W. P. & Ross, A. B. Rate Constants for the Decay and Reactions of the Lowest Electronically Excited Singlet-State of Molecular-Oxygen in Solution — An Expanded and Revised Compilation. *J. Phys. Chem. Ref. Data, Monograph 9, 4th ed.* **24**, 663−1021 (1995).

53 Petit, Y. K. et al. DABCOnium: An Efficient and High-Voltage Stable Singlet Oxygen Quencher for Metal–O_2 Cells. *Angew. Chem. Int. Ed.* **58**, 6535-6539 (2019).

Data availability. The data that support the plots within this paper and other findings of this study are available from the corresponding author S.A.F. upon reasonable request. Source Data for Figs. 2–4 and Extended Data Figs. 2–13 are provided with the paper.

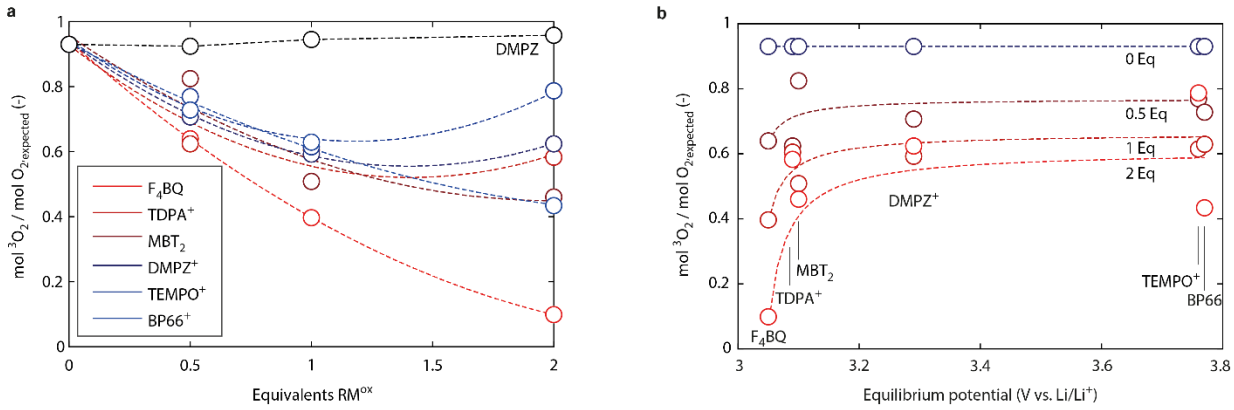

Extended Data Figure 1 | $^3O_2$ loss upon superoxide disproportionation in presence of RM^{ox}. KO_2 powder was immersed in 0.1 M LiTFSI/TEGDME containing 0, 0.5, 1, or 2 equivalents of the indicated RM^{ox}. One equivalent is the amount to theoretically evolve all O_2 (0.5 mol RM^{ox}/mol KO_2) considering 0.5 mol O_2/mol KO_2 to evolve from disproportionation. Equal amounts of electrolytes were used and hence the RM^{ox} concentration adapted. **a**, The found amounts of $^3O_2$ relative to the total amount expected from disproportionation and oxidation for the indicated RM^{ox}. The dashed lines are quadratic polynomial fits. To prove that the RM^{ox} rather than RM^{red} drives $^3O_2$ loss, we also used the reduced form of DMPZ. **b**, The data in a plotted versus the redox potential of the RMs. The trendlines are to guide the eye. See Supplementary Note 7 for in-depth discussion.

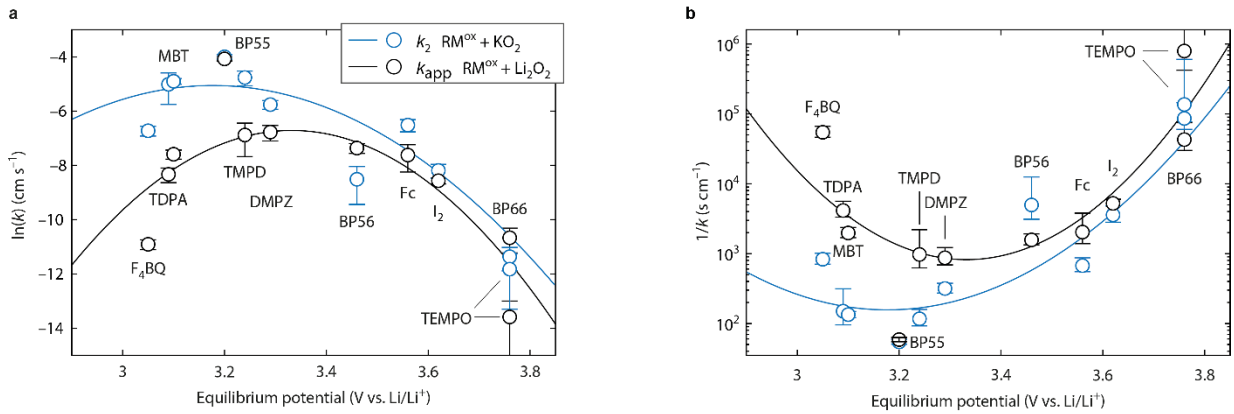

Extended Data Figure 2 | Oxidation kinetics and RM^{ox} concentration. **a**, Comparision of the mediated superoxidation kinetics k_2 and apparent peroxide oxidation kinetics k_{app} including the fits with the Marcus expression in equation (6). **b**, 1/k which is proportional to the required RM^{ox} concentration ($c_{RM^{ox}} = \nu/k$) to drive a certain areal oxidation rate $\nu = k \cdot c_{RM^{ox}}$.